

# We are IntechOpen, the world's leading publisher of Open Access books Built by scientists, for scientists

**4,800**

Open access books available

**122,000**

International authors and editors

**135M**

Downloads

Our authors are among the

**154**

Countries delivered to

**TOP 1%**

most cited scientists

**12.2%**

Contributors from top 500 universities



**WEB OF SCIENCE™**

Selection of our books indexed in the Book Citation Index  
in Web of Science™ Core Collection (BKCI)

Interested in publishing with us?  
Contact [book.department@intechopen.com](mailto:book.department@intechopen.com)

Numbers displayed above are based on latest data collected.

For more information visit [www.intechopen.com](http://www.intechopen.com)



# On the Design of Underactuated Finger Mechanisms for Robotic Hands

Pierluigi Rea

*DiMSAT, University of Cassino  
Italy*

## 1. Introduction

The mechatronic design of robotic hands is a very complex task, which involves different aspects of mechanics, actuation, and control. In most of cases inspiration is taken by the human hand, which is able to grasp and manipulate objects with different sizes and shapes, but its functionality and versatility are very difficult to mimic. Human hand strength and dexterity involve a complex geometry of cantilevered joints, ligaments, and musculotendinous elements that must be analyzed as a coordinated entity. Furthermore, actuation redundancy of muscles generates forces across joints and tissues, perception ability and intricate mechanics complicate its dynamic and functional analyses.

By considering these factors it is evident that the design of highly adaptable, sensor-based robotic hands is still a quite challenge objective giving in a number of cases devices that are still confined to the research laboratory.

There have been a number of robotic hand implementations that can be found in literature. A selection of leading hand designs reported here is limited in scope, addressing mechanical architecture, not control or sensing schemes. Moreover, because this work is concentrated to finger synthesis and design, the thumb description is excluded, as well as two-fingered constructions, because most of them were designed to work as grippers and would not integrate in the frame of multi-finger configuration.

Significant tendon operated hands are the Stanford/JPL hand and the Utah/MIT hand. In particular, the first one has three 3-DOF fingers, each of them has a double-jointed head knuckle providing  $90^\circ$  of pitch and yaw and another distal knuckle with a range of  $\pm 135^\circ$ . The Utah/MIT dextrous hand has three fingers with 4-DOFs, each digit of this hand has a non anthropomorphic design of the head knuckle excluding circumduction. The inclusion of three fingers minimizes reliance on friction and adds redundant support to manipulations tasks. Each  $N$ -DOF finger is controlled by  $2-N$  independent actuators and tension cables. Although these two prototypes exhibit a good overall behaviour, they suffer of limited power transmission capability.

The prototype of the DLR hand possesses special designed actuators and sensors integrated in the hand's palm and fingers. This prototype has four fingers with 3-DOFs each, a 2-DOFs base joint gives  $\pm 45^\circ$  of flexion and  $\pm 30^\circ$  of abduction/adduction, and 1-DOF knuckle with  $135^\circ$  of flexion. The distal joint, which is passively driven, is capable of flexing  $110^\circ$ .

A prototype of an anthropomorphic mechanical hand with pneumatic actuation has been developed at Polytechnic of Turin having 4 fingers with 1-DOF each and it is controlled through PWM modulated digital valves.

Following this latter basic idea, several articulated finger mechanisms with only 1-DOF were designed and built at the University of Cassino and some prototypes allowing to carry out suitable grasping tests of different objects were developed.

More recently, the concept of the underactuation was introduced and used for the design of articulated finger mechanisms at the Laval University of Québec.

Underactuation concept deals with the possibility of a mechanical system to be designed having less control inputs than DOFs. Thus, underactuated robotic hands can be considered as a good compromise between manipulation flexibility and reduced complexity for the control and they can be attractive for a large number of application, both industrial and non conventional ones.

## 2. The underactuation concept

Since the last decades an increasing interest has been focused on the design and control of underactuated mechanical systems, which can be defined as systems whose number of control inputs (i.e. active joints) is smaller than their DOFs. This class of mechanical systems can be found in real life; examples of such systems include, but not limited to, surface vessels, spacecraft, underwater vehicles, helicopters, road vehicles, and robots.

The underactuation property may arise from one of the following reasons:

- the dynamics of the system (e.g. aircrafts, spacecrafts, helicopters, underwater vehicles);
- needs for cost reduction or practical purposes (e.g. satellites);
- actuator failure (e.g. in surface vessel or aircraft).

Furthermore, underactuation can be also imposed artificially to get a complex low-order nonlinear systems for gaining an insight in the control theory and developing new strategies. However, the benefits of underactuation can be extended beyond a simple reduction of mechanical complexity, in particular for devices in which the distribution of wrenches is of fundamental importance. An example is the automobile differential, in which an underactuated mechanism is commonly used to distribute the engine power to two wheels. The differential incorporates an additional DOF to balance the torque delivered to each wheel. The differential fundamentally operates on wheel torques instead of rotations; aided by passive mechanisms, the wheels can rotate along complex relative trajectories, maintaining traction on the ground without closed loop active control.

Some examples found in Robotics can be considered as underactuated systems such as: legged robots, underwater and flying robots, and grasping and manipulation robots.

In particular, underactuated robotic hands are the intermediate solution between robotic hands for manipulation, which have the advantages of being versatile, guarantee a stable grasp, but they are expensive, complex to control and with many actuators; and robotic grippers, whose advantages are simplified control, few actuators, but they have the drawbacks of being task specific, and perform an unstable grasp.

In an underactuated mechanism actuators are replaced by passive elastic elements (e.g. springs) or limit switches. These elements are small, lightweight and allow a reduction in the number of actuators. They may be considered as passive elements that increase the adaptability of the mechanism to shape of the grasped object, but can not and should not be handled by the control system.

The correct choice of arrangement and the functional characteristics of the elastic or mechanical limit (mechanical stop) ensures the proper execution of the grasping sequence. In a generic sequence for the grasping action, with an object with regular shape and in a fixed position, one can clearly distinguish the different phases, as shown in Fig. 1.

In Fig.1a the finger is in its initial configuration and no external forces are acting. In Fig.1b the proximal phalanx is in contact with the object. In the Fig.1c the middle phalanx, after a relative rotation respect to the proximal phalanx, starts the contact with the object. In this configuration, the first two phalanges can not move, because of the object itself. In Fig.1d, finally, the finger has completed the adaptation to the object, and all the three phalanges are in contact with it. A similar sequence can be described for an irregularly shaped object, as shown in Fig.2, in which it is worth to note the adaptation of the finger to the irregular object shape.

An underactuated mechanism allows the grasping of objects in a more natural and more similar to the movement obtained by the human hand. The geometric configuration of the finger is automatically determined by external constraints related with the shape of the object and does not require coordinated activities of several phalanges. It is important to note that the sequences shown in Figs.1 and 2 can be obtained with a continuous motion given by a single actuator.

Few underactuated finger mechanisms for robotic hands have been proposed in the literature. Some of them are based on linkages, while others are based on tendon-actuated mechanisms. Tendon systems are generally limited to rather small grasping forces and they lead to friction and elasticity. Hence, for applications in which large grasping forces are

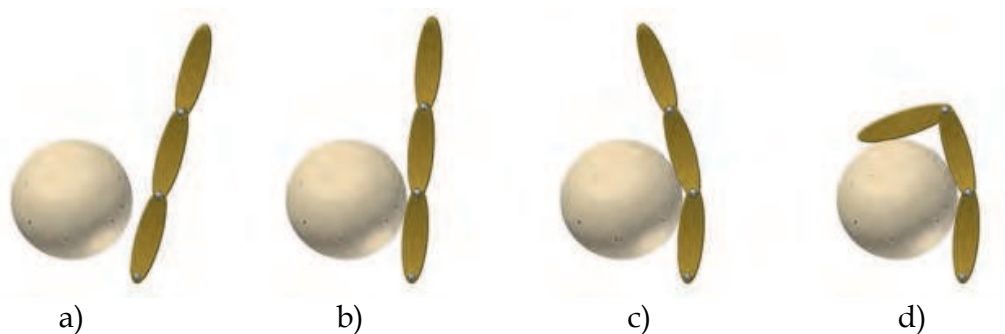


Fig. 1. A sequence for grasping a regularly shaped object: a) starting phase; b) first phalange is in its final configuration; c) second phalange is in its final configuration; d) third phalange is in its final configuration.

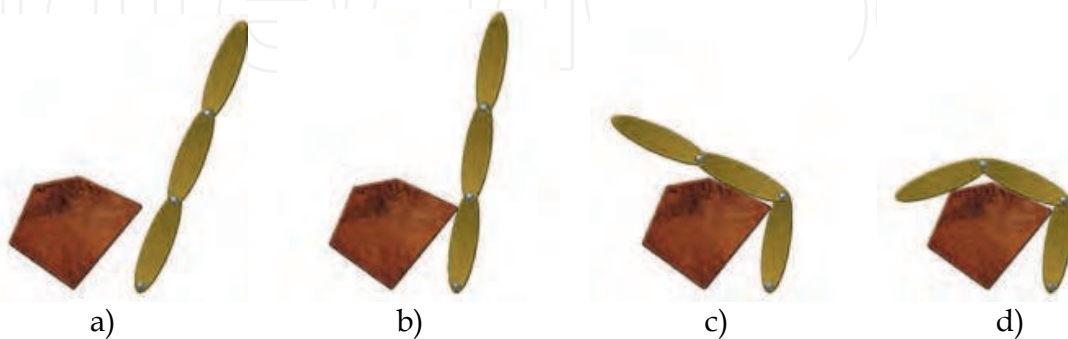


Fig. 2. A sequence for grasping an irregularly shaped object: a) starting phase; b) first phalange is in its final configuration; c) second phalange is in its final configuration; d) third phalange is in its final configuration.

required, linkage mechanisms are usually preferred and this Chapter is focused to the study of the latter type of mechanisms.

An example of underactuation based on cable transmission is shown in Fig.3a, it consists of a cable system, which properly tensioned, act in such a way as to close the fingers and grasp the object.

The underactuation based on link transmission, or linkages, consists of a mechanism with multiple DOFs in which an appropriate use of passive joints enables to completely envelop the object, so as to ensure a stable grasp. An example of this system is shown in Fig.3.b. This type solution for robotic hands has been developed for industrial or space applications with the aim to increase functionality without overly complicating the complexity of the mechanism, and ensuring a good adaptability to the object in grasp.

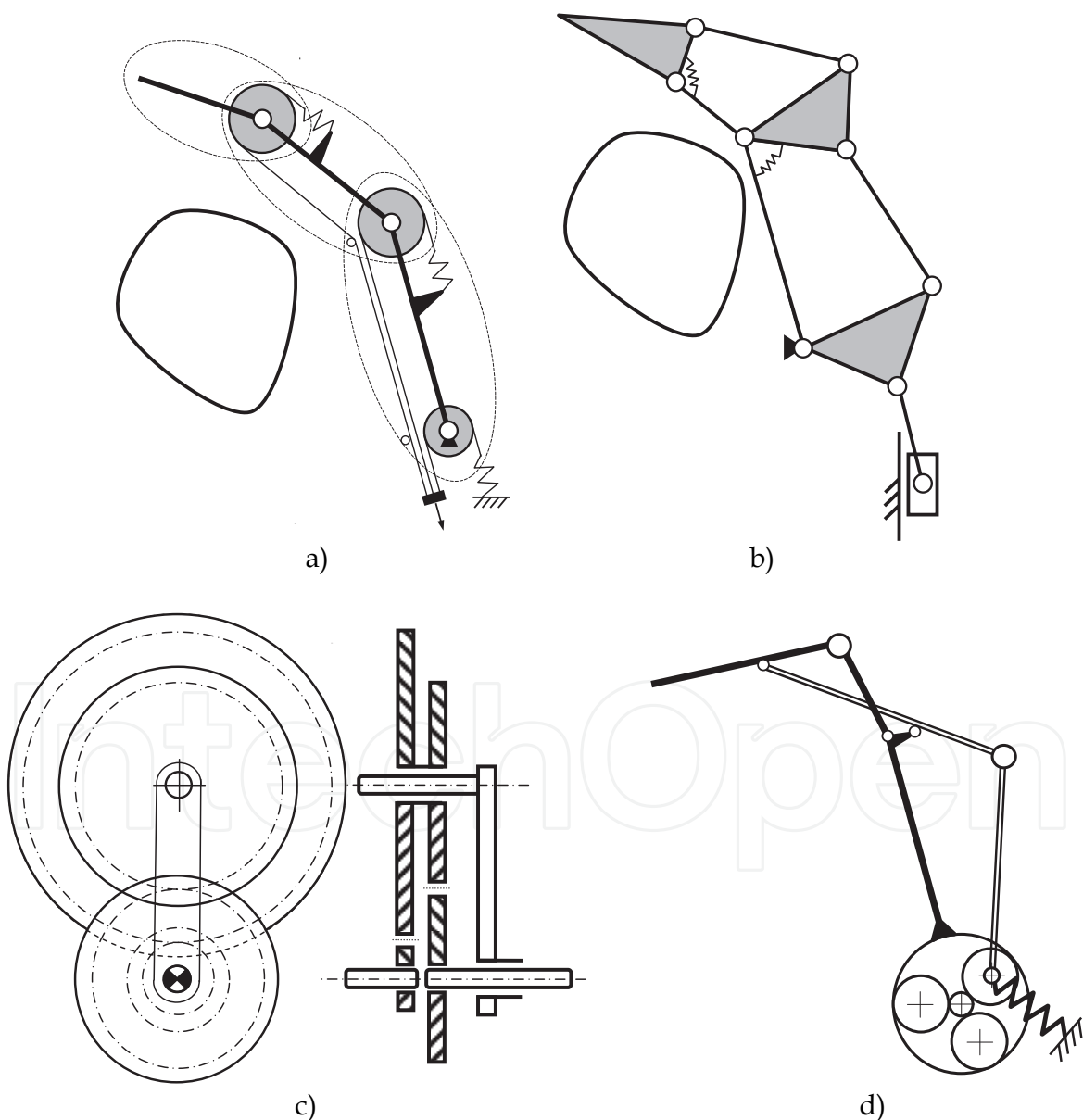


Fig. 3. Examples of underactuation systems: a) tendon-actuated mechanism; b) linkage mechanism; c) differential mechanism; d) hybrid mechanism.



A differential mechanism, shown in Fig. 3c, is a device, usually but not necessarily used for gears, capable of transmitting torque and rotation through three shafts, almost always used in one of two ways: in one way, it receives one input and provides two outputs, this is found in most automobiles, and in the other way, it combines two inputs to create an output that is the sum, difference, or average, of the inputs. These differential mechanisms have unique features like the ability to control many DOFs with a single actuator, mechanical stops or elastic limits. The differential gear, commonly used in cars, distributes the torque from the engine on two-wheel drive according to the torque acting on the wheels. Applying this solution to robotic hands, the actuation can be distributed to the joints according to the reaction forces acting to each phalanx during its operation.

Hybrid solutions have been also developed and make use of planetary gears and linkages, together with mechanical stops or elastic elements. An example is shown in Fig. 3d.

### 3. Design of underactuated finger mechanism

An anthropomorphic robotic finger usually consists of 2-3 hinge-like joints that articulates the phalanges. In addition to the pitch enabled by a pivoting joint, the head knuckle, sometimes also provides yaw movement. Usually, the condyloid nature of the human metacarpal-phalangeal joint is often separated into two rotary joints or, as in the case under-study, simplified as just one revolute joint.

Maintaining size and shape of the robot hand consistent to the human counterpart is to facilitate automatic grasp and sensible use of conventional tools designed for human finger placement. This holds true for many manipulative applications, especially in prosthesis and tele-manipulation where accuracy of a human hand model enables more intuitive control to the slave. Regarding to the actuation system in most of cases adopted solutions do not attempt to mimic human capabilities, but assume some of the pertinent characteristics of the force generation, since complex functionality of tendons and muscles that have to be replaced and somehow simplified by linear or revolute actuators and rotary joints.

The design of a finger mechanism proposed here uses the concept of underactuation applied to mechanical hands. Specifically, underactuation allows the use of  $n - m$  actuators to control  $n$ -DOFs, where  $m$  passive elastic elements replace actuators, as shown in Fig. 4. Thus, the concept of underactuation is used to design a suitable finger mechanism for mechanical hands, which can automatically envelop objects with different sizes and shapes through simple stable grasping sequences, and do not require an active coordination of the phalanges. Referring to Figs. 4 and 5, the underactuated finger mechanism of Ca.U.M.Ha. (Cassino-Underactuated-Multifinger-Hand) is composed by three links  $m_j$  for  $j = 1, 2, 3$ , which correspond to the proximal, median and distal phalanges, respectively. Dimensions of the simplified sketch reported in Fig.4 have been chosen according to the overall characteristics of the human finger given in Table 1. In particular, in Fig. 4,  $\theta_{iM}$  are the maximal angles of rotation, and torsion springs are denoted by  $S_1$  and  $S_2$ . In the kinematic scheme of Fig.5, two four-bar linkages  $A, B, C, D$  and  $B, E, F, G$  are connected in series through the rigid body  $B, C, G$ , for transmitting the motion to the median and distal phalanges, respectively, where the rigid body  $A, D, P$  represents the distal phalange. Likewise to the human finger, links  $m_j$  ( $j = 1, 2, 3$ ) are provided of suitable mechanical stoppers in order to avoid the hyper-extension and hyper-flexion of the finger mechanism. Both revolute joints in  $A$  and  $B$  are provided of torsion springs in order to obtain a statically determined system in each configuration of the finger mechanism.

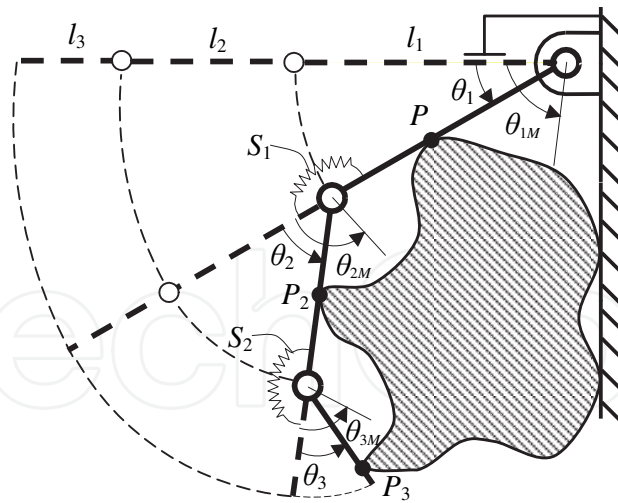


Fig. 4. Simplified sketch of underactuated finger mechanism.

Phalanx	Length	Angle
$m_1$	$l_1 = 43 \text{ mm}$	$\theta_{1M} = 83^\circ$
$m_2$	$l_2 = 25 \text{ mm}$	$\theta_{2M} = 105^\circ$
$m_3$	$l_3 = 23 \text{ mm}$	$\theta_{3M} = 78^\circ$

Table 1. Characteristics of an index human finger.

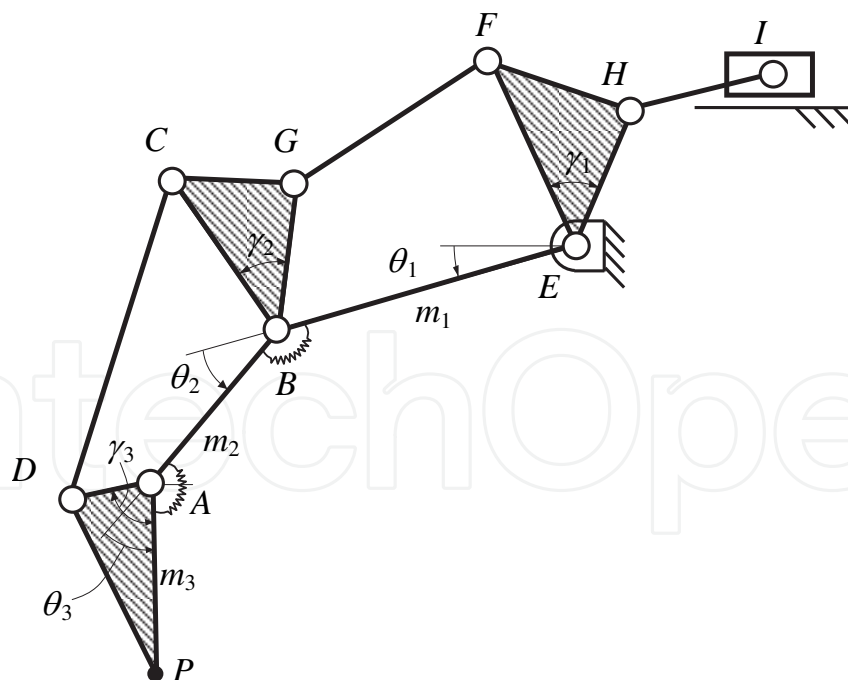


Fig. 5. Kinematic sketch of the underactuated finger mechanism.

**3.1 Optimal kinematic synthesis**

The optimal dimensional synthesis of the function-generating linkage shown in Fig. 5, which is used as transmission system from the pneumatic cylinder to the three phalanges of

the proposed underactuated finger mechanism, is formulated by using the Freudenstein's equations and the transmission defect, as index of merit of the force transmission. The three linkages connected in series are synthesized as in the following by starting from the four-bar linkage, which moves the third phalanx.

### 3.1.1 Synthesis of the four bar linkage A, B, C, D

By considering the four-bar linkage  $A, B, C, D$  in Fig. 5, one has to refer to Fig.6 and the Freudenstein's equations can be expressed in the form

$$R_1 \cos \varepsilon_i - R_2 \cos \rho_i + R_3 = \cos(\varepsilon_i - \rho_i) \quad i = 1, 2, 3 \quad (1)$$

with

$$R_1 = l_2 / a; \quad R_2 = l_2 / c; \quad R_3 = (a^2 - b^2 + c^2 + l_2^2) / 2ac \quad (2)$$

where  $l_2$  is the length of the second phalanx,  $a, b$  and  $c$  are the lengths of the links  $AD, DC$  and  $CB$  respectively, and  $\varepsilon_i$  and  $\rho_i$  for  $i = 1, 2, 3$  are the input and output angles of the four-bar linkage  $ABCD$ .

Equations (1) can be solved when three positions 1), 2) and 3) of both links  $BC$  and  $AD$  are given through the pairs of angles  $(\varepsilon_i, \rho_i)$  for  $i = 1, 2, 3$ . According to a suitable mechanical design of the finger, (zoomed view reported in Fig.7) some design parameters are assumed, such as  $\alpha = 50^\circ$  for the link  $AD$ ,  $\gamma = 40^\circ$  and  $\beta_1 = 25^\circ$  for the link  $BC$ , the pairs of angles  $(\varepsilon_1 = 115^\circ, \rho_1 = 130^\circ)$  and  $(\varepsilon_3 = 140^\circ, \rho_3 = 208^\circ)$  are obtained for the starting 1) and final 3) configurations respectively. Angle  $\rho_3$  is given by the sum of  $\rho_1$  and  $\theta_{3M}$ . Since only two of the three pairs of angles required by the Freudenstein's equations are assigned as design specification of the function-generating four-bar linkage  $ABCD$ , an optimization procedure in terms of force transmission has been developed by assuming  $(\varepsilon_2, \rho_2)$  as starting values of the optimization, which correspond to both middle positions between 1) and 3) of links  $BC$  and  $AD$  respectively.

The transmission quality of the four-bar linkage is defined as the integral of the square of the cosine of the transmission angle. The complement of this quantity is defined "transmission defect" by taking the form

$$z' = \frac{1}{\varepsilon_3 - \varepsilon_1} \int_{\varepsilon_1}^{\varepsilon_3} \cos^2 \mu_1 d\varepsilon \quad (3)$$

where the transmission angle  $\mu_1$  is expressed as

$$\mu_1 = \cos^{-1} \left( \frac{l_2^2 + c^2 - a^2 - b^2 - 2l_2 c \cos(\pi - \varepsilon)}{2ab} \right) \quad (4)$$

The optimal values of the pair of angles  $(\varepsilon_2, \rho_2)$  are obtained through the optimization of the transmission defect  $z'$ . In particular, the outcome of the computation has given  $(\varepsilon_2 = 132.5^\circ, \rho_2 = 180.1^\circ)$  and consequently,  $a = 22.6$  mm,  $b = 58.3$  mm and  $c = 70.9$  mm have been obtained from the Eqs.(1) and (2).

It is worth to note that, as reported from Fig.8a to Fig.8c, these plots give many design solutions, the choice can be related to the specific application and design requirements. In



the case under-study parameters  $\varepsilon_2$  and  $\rho_2$  have been obtained in order to have the maximum of the mean values for the transmission angle. The transmission angle  $\mu_1$  versus the input angle  $\varepsilon$  for the synthesized mechanism is shown in Fig.8d.

Figure 8 , shows a parametric study of the  $a, b, c$ , parameters as function of  $\varepsilon_2$  and  $\eta_2$ . The colour scale represents the relative link length. For each plot the circle represents the choice that has been made for  $\varepsilon_2$  and  $\rho_2$ , by assuming the length  $a = 23$  mm, for the case under-study.

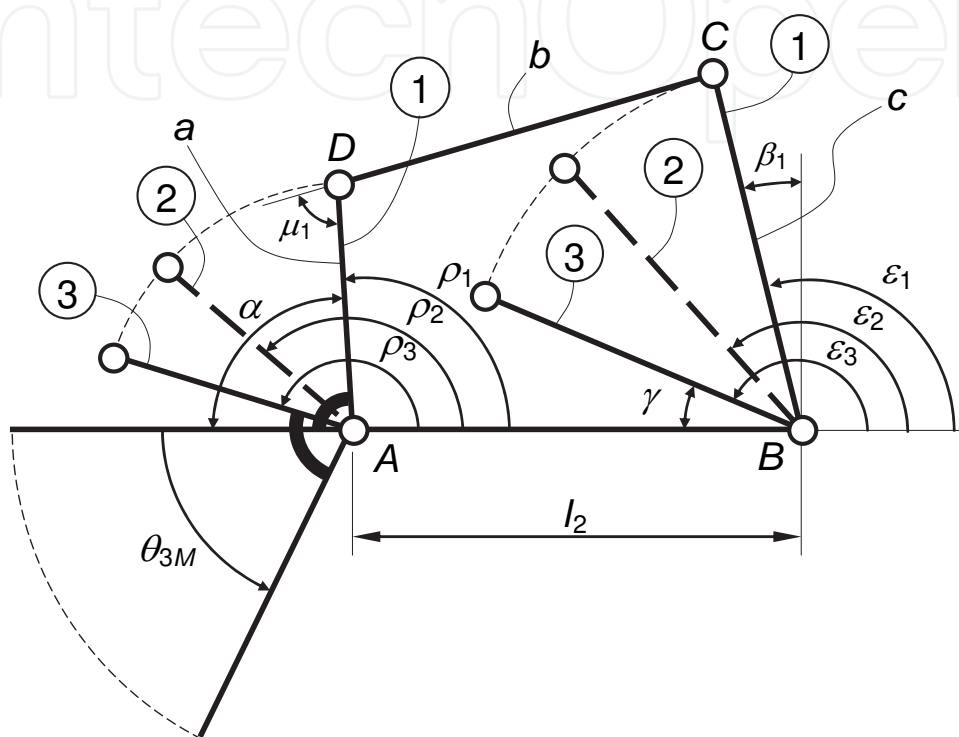


Fig. 6. Sketch for the kinematic synthesis of the four bar linkage  $ABCD$ , shown in Fig. 5.

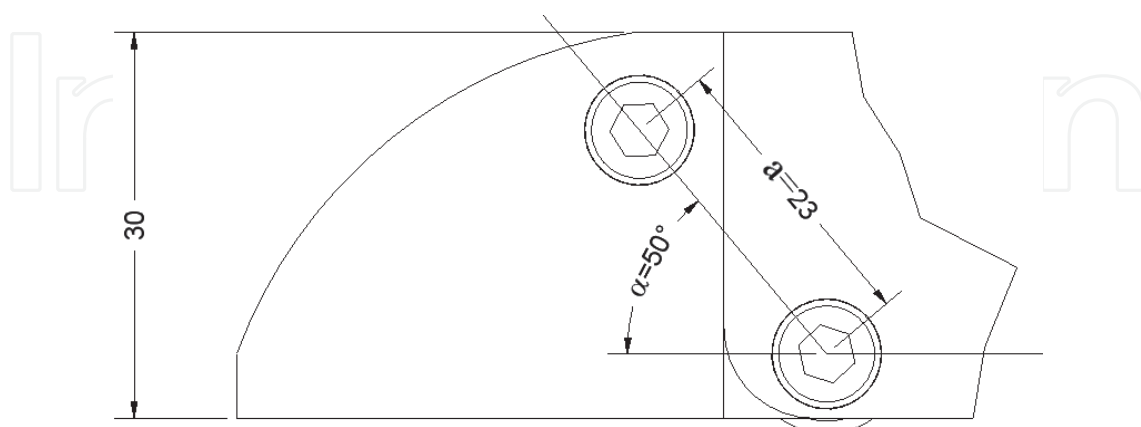


Fig. 7. Mechanical design of a particular used to define the angle  $\alpha$  and the link length  $a$  of  $A, B, C, D$ , in Fig. 6.

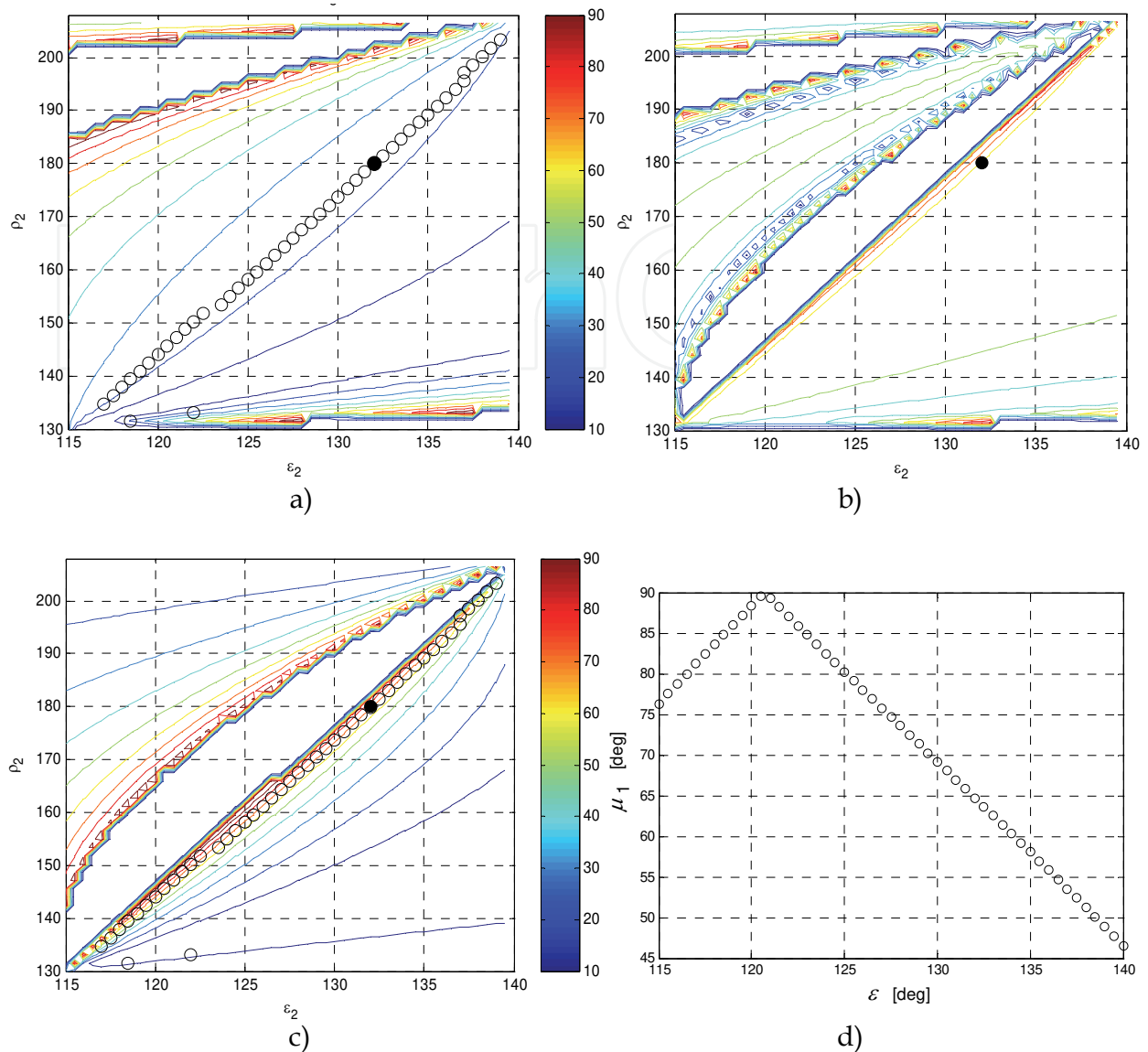


Fig. 8. Map of the link length versus the angles  $\epsilon_2$  and  $\rho_2$ ; a) link  $AD$ , b) link  $DC$ ; c) link  $BC$ , d) Transmission angle  $\mu_1$  versus angle  $\epsilon$  for the moving link  $c$ .

### 3.1.2 Synthesis of the four-bar linkage B, E, F, G

The same method has been applied to the synthesis of the function-generating four-bar linkage  $BEFG$ . In fact, referring to Fig.9, the Freudenstein's equations can be expressed in the form

$$R_1 \cos \psi_i - R_2 \cos \varphi_i + R_3 = \cos(\psi_i - \varphi_i) \quad i = 1, 2, 3 \tag{5}$$

with

$$R_1 = l_1 / d; R_2 = l_1 / f; R_3 = (d^2 - e^2 + f^2 + l_1^2) / 2df \tag{6}$$

where  $l_1$  is the length of the first phalanx,  $d$ ,  $e$  and  $f$  are lengths of the links  $BG$ ,  $GF$  and  $FE$  respectively, and  $\psi_i$  and  $\varphi_i$  for  $i = 1, 2, 3$  are the input and output angles of the four-bar linkage  $BEFG$ .

Likewise to the four-bar linkage  $ABCD$ , Eqs.(5) can be solved when three positions 1), 2) and 3) of both links  $EF$  and  $BG$  are given through the pairs of angles  $(\psi_i, \varphi_i)$  for  $i = 1, 2, 3$ . In particular, according to a suitable mechanical design of the finger, the design parameters  $\gamma = 40^\circ$ ,  $\beta_2 = 30^\circ$  and  $\delta = 10^\circ$  are assumed empirically. Consequently, the pairs of angles  $(\psi_1 = 80^\circ, \varphi_1 = 60^\circ)$  and  $(\psi_3 = 140^\circ, \varphi_3 = 190^\circ)$  are obtained for the starting 1) and final 3) positions of both links  $EF$  and  $BG$ .

Since only two of the three pairs of angles required by the Freudenstein's equations are assigned as design specification of the function-generating four-bar linkage  $BEFG$ , an optimization procedure in terms of force transmission has been carried out by assuming  $(\psi_2, \varphi_2)$  as starting values of the optimization the middle positions between 1) and 3) of links  $EF$  and  $BG$  respectively. The transmission defect  $z'$  of the function-generating four-bar linkage  $BEFG$  takes the form

$$z' = \frac{1}{\psi_3 - \psi_1} \int_{\psi_1}^{\psi_3} \cos^2 \mu_2 d\psi \quad (7)$$

where the transmission angle  $\mu_2$  is expressed as

$$\mu_2 = \cos^{-1} \left( \frac{l_1^2 + f^2 - d^2 - e^2 - 2l_1 f \cos(\pi - \psi)}{2de} \right) \quad (8)$$

The optimal values of the pair of angles  $(\psi_2, \varphi_2)$  are obtained and the output of the computation gives  $(\psi_2 = 115.5^\circ, \varphi_2 = 133.7^\circ)$ . Consequently,  $d = 53.4$  mm,  $e = 96.3$  mm and  $f = 104.9$  mm have been obtained from Eqs.(5) and (6). Figure 10, shows a parametric study of the  $d, e, f$ , parameters as a function of  $\psi_2$  and  $\varphi_2$ . The colour scale represents the relative link length. For each plot the circle represents the choice that has been made for  $\psi_2$  and  $\varphi_2$ , for the case under study. The diagram of the transmission angle  $\mu_2$  versus the input angle  $\psi$  of the moving link  $EF$  of the synthesized mechanism  $BEFG$  is shown in Fig. 10d.

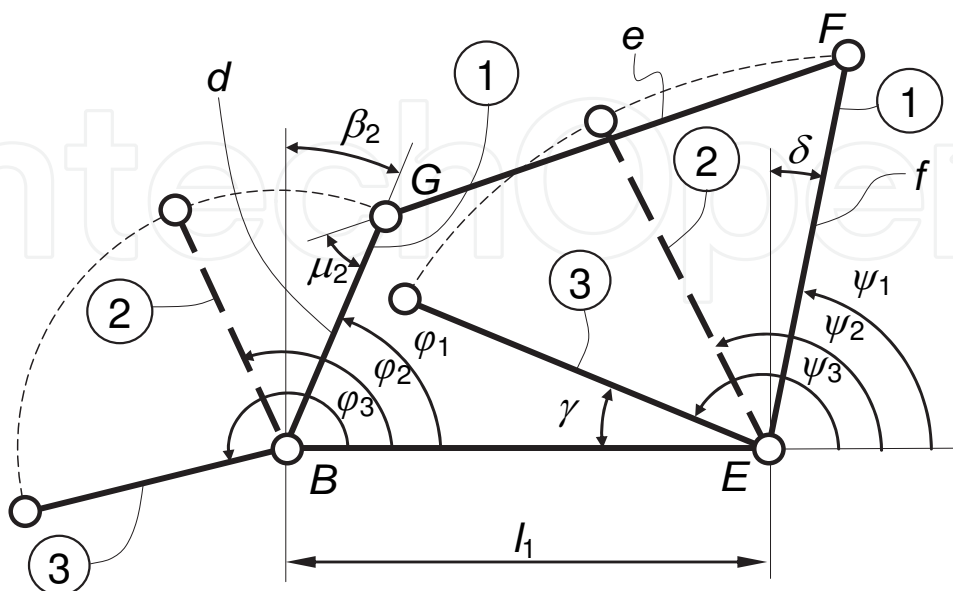


Fig. 9. Sketch for the kinematic synthesis of the four-bar linkage  $BEFG$ .

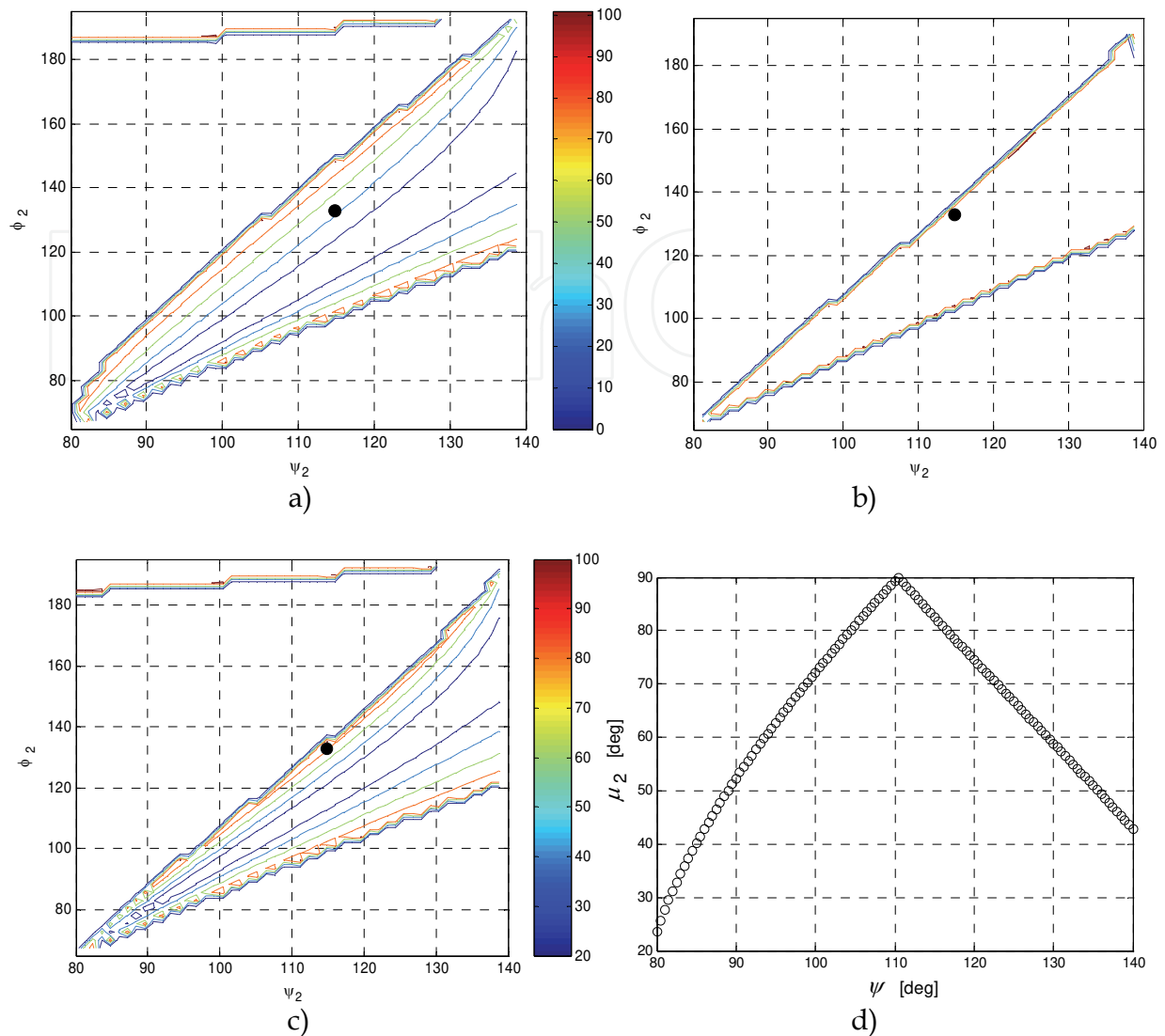


Fig. 10. Map of the link length versus the angles  $\psi_2$  and  $\phi_2$ ; a) link BG, b) link GF, c) link EF, d) transmission angle  $\mu_2$  versus angle  $\psi$  of the moving link EF.

### 3.1.3 Synthesis of the slider-crank mechanism EHI

Likewise to both four-bar linkages  $ABCD$  and  $BEFG$ , the offset slider-crank mechanism  $EHI$  of Fig. 11 is synthesized by using the Freudenstein's equations, which takes the form

$$R_1 (s_1 - x_i) \cos \lambda_i + R_2 \sin \lambda_i - R_3 = (s_1 - x_i)^2 \quad i = 1, 2, 3 \quad (9)$$

with

$$\begin{aligned} R_1 &= 2g; \\ R_2 &= 2g o_f; \\ R_3 &= g^2 + o_f^2 - h^2 \end{aligned} \quad (10)$$

where  $o_f$  is the offset,  $g$  and  $h$  are the lengths of the links  $EH$  and  $HI$  respectively, and  $x_i$  and  $\lambda_i$  for  $i = 1, 2, 3$  are the input displacement of the piston and the output rotation angle of the

link  $EH$  of the slider-crank mechanism  $EHI$ . Equations (9) can be solved when three positions 1), 2) and 3) of both piston and link  $EH$  are given through the pairs of parameters  $(x_i, \lambda_i)$  for  $i = 1, 2, 3$ . In particular, according to a suitable mechanical design of the finger, the design parameters  $(x_1 = 0 \text{ mm}, \lambda_1 = 37^\circ)$  and  $(x_3 = 75 \text{ mm}, \lambda_3 = 180^\circ)$  are assumed empirically for the starting 1) and final 3) positions of both piston and link  $EH$ . The optimization procedure in terms of force transmission has been carried out by assuming as starting values of the optimization the middle position between 1) and 3) of the piston and link  $EH$  respectively. The transmission defect  $z'$  of the function-generating slider-crank mechanism  $EHI$  takes the form

$$z' = \frac{1}{x_3 - x_1} \int_{x_1}^{x_3} \cos^2 \mu_3 \, dx \quad (11)$$

where the transmission angle  $\mu_3$  is expressed as

$$\mu_3 = \cos^{-1} \left( \frac{(s_1 - x)^2 + o_f^2 - g^2 - h^2}{2gh} \right) \quad (12)$$

The optimal values of the pair of parameters  $(x_2, \lambda_2)$  are obtained, and the outcome of the computation has given  $(x_2 = 47.5 \text{ mm}, \lambda_2 = 126.9^\circ)$ . Consequently,  $o_f = 43.4 \text{ mm}$ ,  $g = 35.7 \text{ mm}$  and  $h = 74.7 \text{ mm}$  have been obtained from the Eqs. (9) and (10).

Figures 12a, 12b and 12c, show a parametric study of the parameters  $g$ ,  $h$  and  $o_f$ , as a function of  $\lambda_2$  and  $s_2$ . The colour scale represents the relative link length and for each plot the marked circle represents the choice that has been made for values  $\lambda_2$  and  $s_2$ . The diagram of the transmission angle  $\mu_3$  versus the input displacement  $x$  of the moving piston of the synthesized slider-crank mechanism  $EHI$  is shown in Fig. 12d.

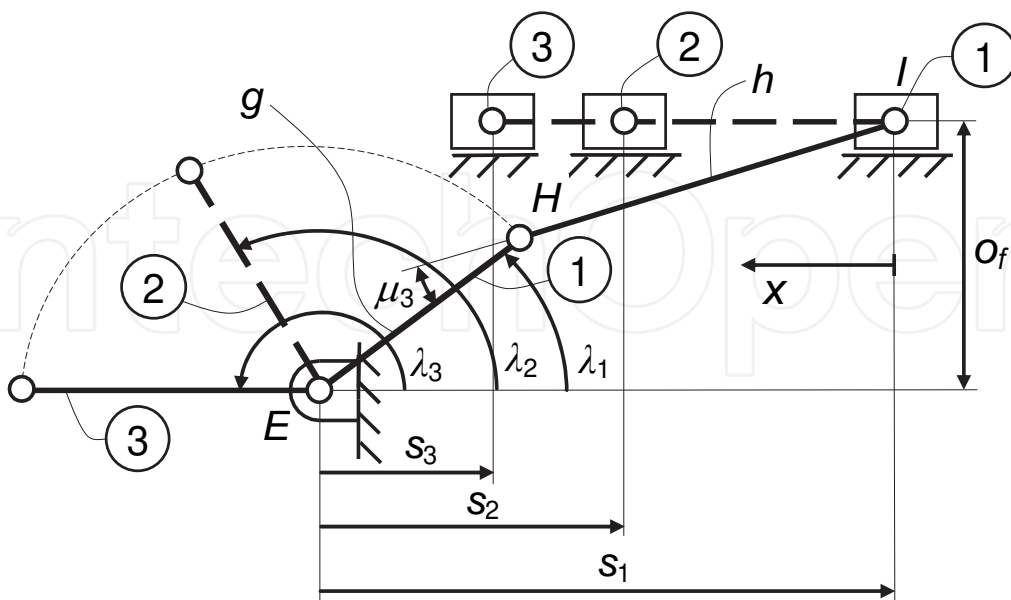


Fig. 11. Kinematic scheme of the offset slider-crank mechanism  $EHI$ .

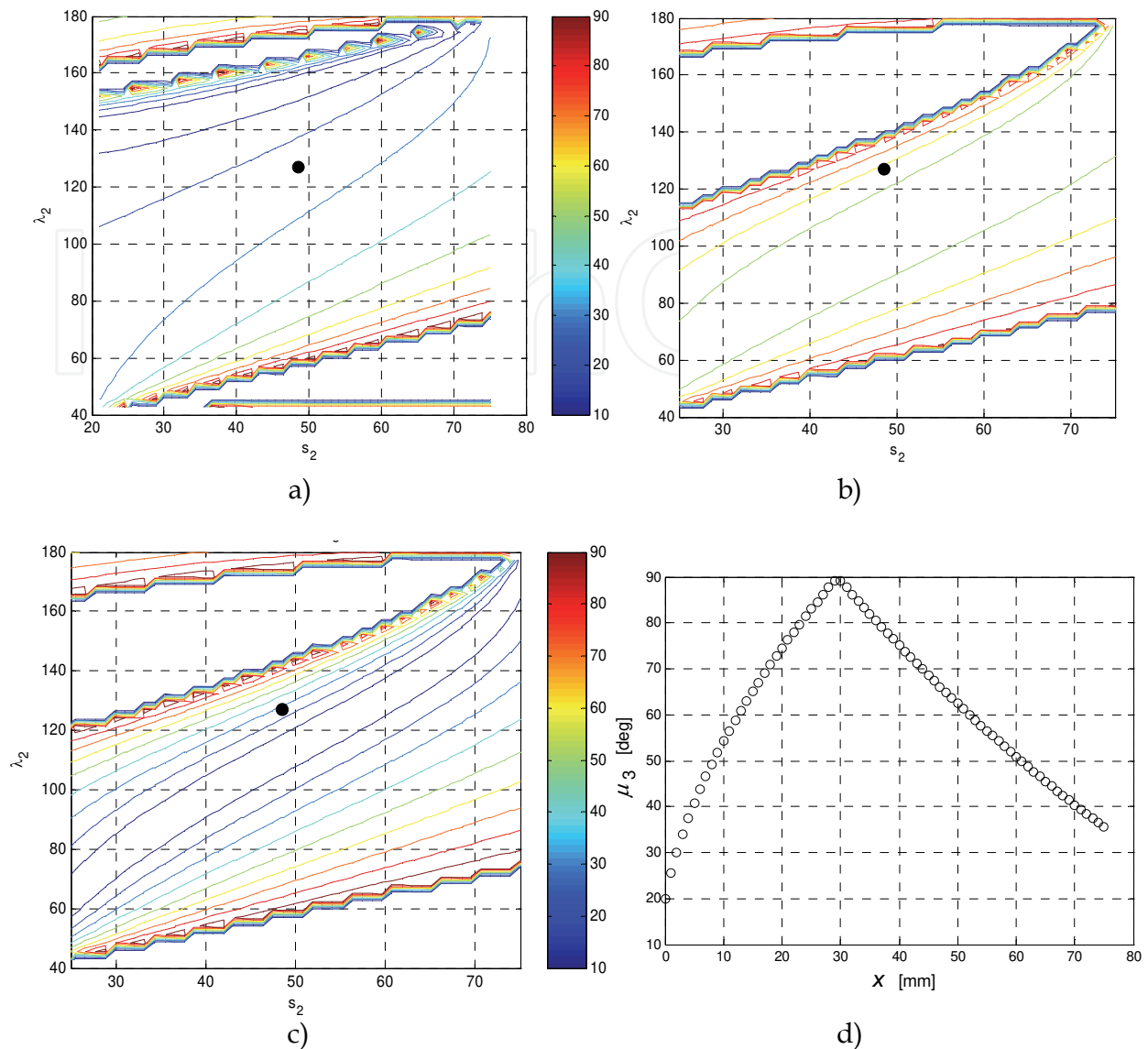


Fig. 12. Map of the link length versus angles  $\lambda_2$  and  $s_2$ ; a) link EI, b) link HI, c) link EH, d) transmission angle  $\mu_3$  versus distance  $x$  of the moving link.

### 3.2 Mechanical design

Figure 13 shows a drawing front view of the designed underactuated finger mechanism. In particular, *EHI* indicates the slider-crank mechanism, *ABCD* indicates the first four-bar linkage, and *DEFG* indicates the second four-bar linkage. In order to obtain the underactuated finger mechanism, two torsion springs ( $S_1$  and  $S_2$ ) have been used at joints *A* and *B* and indicated with 1 and 2, respectively.

Aluminium has been selected for its characteristics of lightness and low-cost. It has the disadvantage of low hardness, therefore for the manufacturing of the revolute joints, ferrules have been considered. In particular, in Fig. 13, it is possible to note that the finger mechanism, which allows the finger motion, is always on the upper side of the phalanges. This is to avoid mechanical interference between the object in grasp and the links' mechanism. Furthermore, the finger is asymmetric, this is due to the fact that is necessary to have a suitable side to mount the torsion spring.



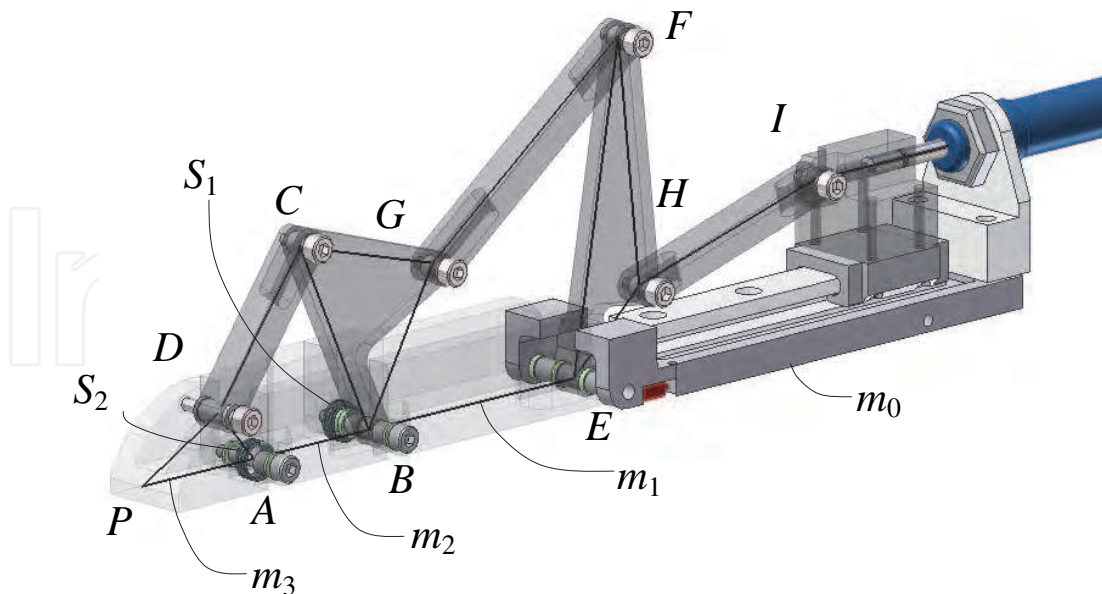


Fig. 13. Mechanical design of the underactuated finger.

Each phalange has a flat surface to interact with the object to be grasped. This is to further consider force sensors to develop a suitable force control of the robotic hand prototype, as reported in Section 4.

The common operation of the four underactuated fingers gives an additional auto-adaptability of the Ca.U.M.Ha. robotic hand, because each finger can reach a different closure configuration according to the shape and size of the object to grasp. This behaviour is due to the uniform distribution of the air pressure inside the pneumatic tank and pushing chambers, as it will be described below.

### 3.3 Actuation and control

The lay-out of the electro-pneumatic circuit of the proposed closed-loop pressure control system is sketched in Fig.14, where the pressure  $P_{OUT}$  in the rigid tank is controlled by means of two PWM modulated pneumatic digital valves  $V_1$  and  $V_2$ , which are connected in supply, at the supply pressure  $P_s$ , and in exhaust, at the atmospheric pressure  $P_A$ , respectively.

Thus, both valves  $V_1$  and  $V_2$  approximate the behaviour of a three-way flow proportional valve, which allows the pressure regulation in the tank. These valves are controlled through the voltage control signals  $V_{PWM1}$  and  $V_{PWM2}$ , which are modulated in PWM at 24 V, as it is required by the valves  $V_1$  and  $V_2$ . These signals are given by a specific electronic board supplied at 24 V, which allows the generation of both signals  $V_{PWM1}$  and  $V_{PWM2}$  and the amplification at 24 V from the input signal  $V_{PWM}$  that lies within the range of  $[-5; +5]$  V. The PWM modulated control signal  $V_{PWM}$  is generated via software because of a suitable Lab-View program.

The feed-back signal  $V_{F/B}$  is given by the pressure transducer  $Tp$  with static gain  $K_T = 1$  V/bar, which is installed on the rigid tank directly.

Thus, a typical PID compensation of the  $\varepsilon$  error between the input electric signal  $V_{SET}$  and the feed-back electric signal  $V_{F/B}$  is carried out through a PC controller, which is provided of the electronic board PCI 6052-E and a terminal block SCB-68.

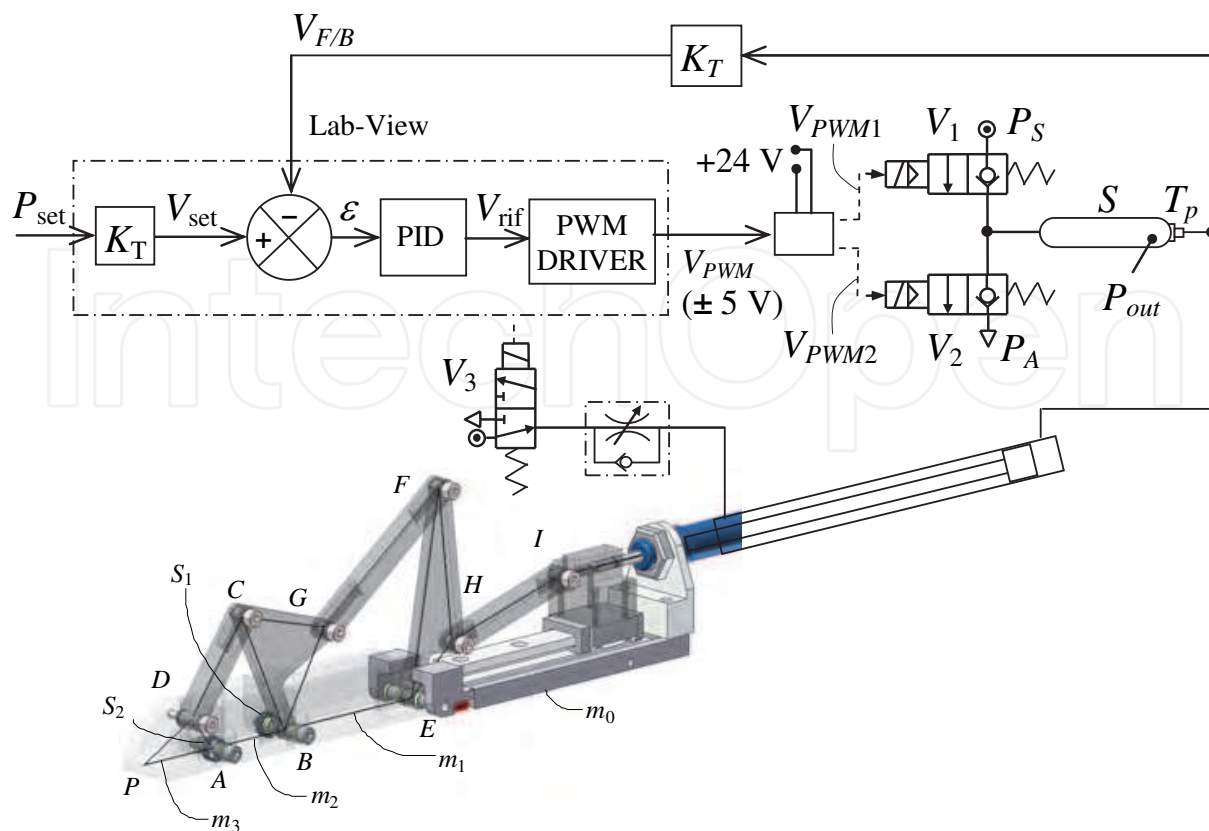


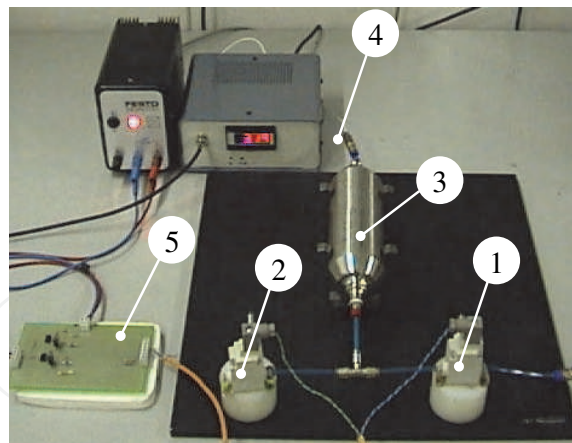
Fig. 14. Scheme for the pressure control of the robotic hand prototype finger.

### 3.3.1 Experimental test-bed

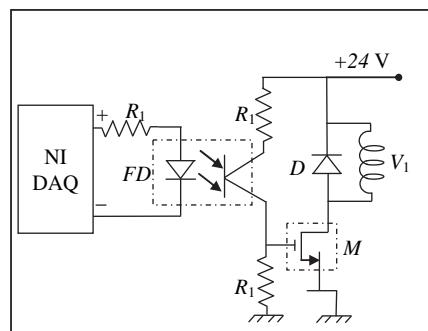
The closed-loop pressure control system and a test bed of Fig.15 have been designed and built according to the scheme of Fig.14. In particular, this test-bed is mainly composed by: 1) and 2), two 2/2 (two-way/two-position) pneumatic digital valves of type SMC VQ21A1-5Y0-C6-F-Q; 3) a tank of type Festo with a volume of 0.4 lt; 4) a pressure transducer of type GS Sensor XPM5-10G, connected to an electronic board of type PCI 6052-E with the terminal block SCB-68, which is connected to the PC in order to generate the control signal  $V_{PWM}$ ; 5) a specific electronic board to split and amplify at 24 V the control signals  $V_{PWM1}$  and  $V_{PWM2}$ .

The electronic circuit of Fig.15b splits and amplifies the modulated electric signal  $V_{PWM}$  that comes from the PWM driver into the signals  $V_{PWM1}$  and  $V_{PWM2}$ , which control the digital valves  $V_1$  and  $V_2$  respectively. This circuit is composed by a photodiode  $FD$ , three equal electric resistors  $R_1$ , a MOSFET  $M$  and a diode  $D$ . In fact, the working range of the electronic board NI DAQ AT MIO-16E-2 is amplified from  $[-5 / +5]$  V to the working range  $[0 / +24]$  V of the digital valves because of the electric supply at 24 V DC. Moreover, this signal is decomposed and sent alternatively to  $V_1$  and  $V_2$  because of the effects of the MOSFET  $M$ .

A suitable software in the form of virtual instrument has been conceived and implemented by using the Lab-View software, as shown in Fig.16. This solution gives the possibility of using the electronic board NI DAQ PCI-6052-E for driving the PWM modulated pneumatic digital valves and acquiring both voltage signals  $V_{SET}$  and  $V_{F/B}$  of the proposed closed-loop pressure control system. Thus, the program can be considered as composed by three main blocks, where the first is for acquiring analogical signals through a suitable scan-rate, the second gives the PID compensation of the pressure error and the third one is for generating the PWM signal.



a)



b)

Fig. 15. Test-bed a) of the proposed closed-loop pressure control system and b) a scheme of the electronic circuit.

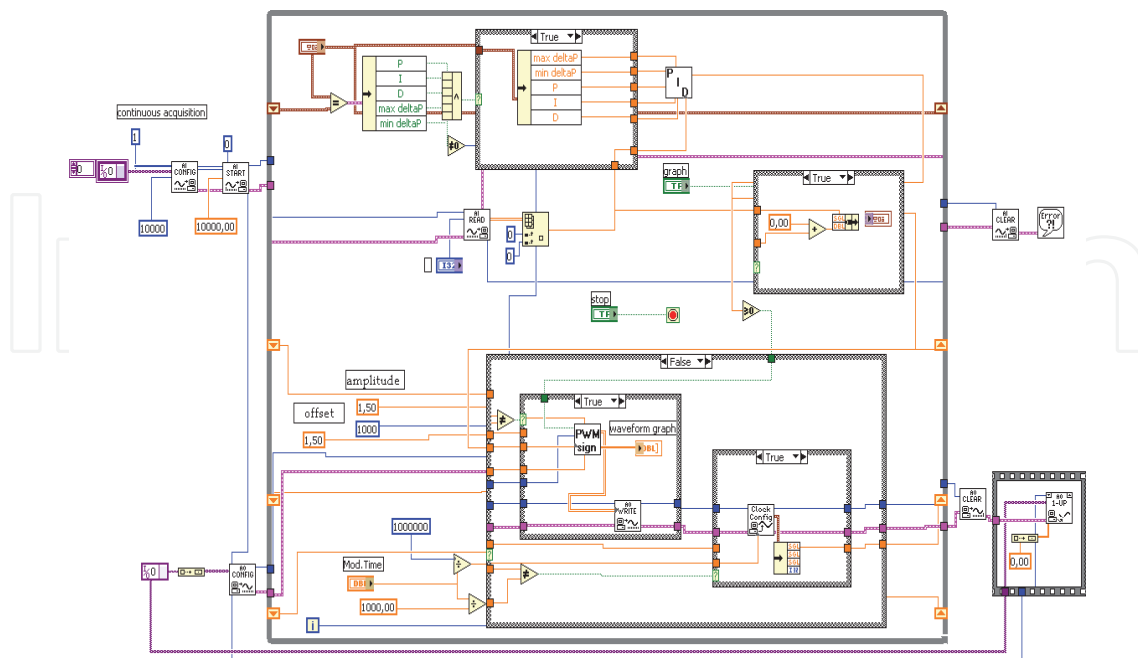


Fig. 16. Lab-View program for controlling the pressure in the tank through PWM modulated pneumatic digital valves.

### 3.3.2 Experimental results

The static and dynamic performances of the proposed closed-loop pressure control system have been analyzed by using the test-bed of Fig.15. Some experimental results in the time domain are reported in Fig.17 in order to show the effects of the proportional gain  $K_p$  of the PID compensator. In particular, the reference and output pressure signals  $P_{SET}$  and  $P_{OUT}$  are compared by increasing the values of the proportional gain  $K_p$  from 0.3 to 2.4, as shown in Figs.17a to 17d, respectively. Taking into account that the pressure transducer  $T_p$  is characterized by a static gain  $K_T = 1$  V/bar, the pressure diagrams of  $P_{SET}$  and  $P_{OUT}$  show the same shape and values of the correspondent voltage diagrams  $V_{SET}$  and  $V_{FB}$ , respectively. Moreover, the diagram of Fig.17c shows a good behaviour at high values of  $K_p$ , even if some instability of the system may appear, as shown in Fig.17d for  $K_p = 2.4$ . The experimental closed-loop frequency response of the proposed pressure control system has been carried out by using a Gain-Phase-Analyzer of type SI 1253. The Bode diagrams of Fig.18a and 18b have been obtained for the periods of the PWM modulation,  $T = 50$  ms and  $T = 100$  ms, respectively. Thus, the diagrams of the pressure signals  $P_{SET}$  and  $P_{OUT}$  versus time, which have been acquired through the Lab-View Data-Acquisition-System, are shown in continuous and dash-dot lines, respectively. In particular, Figs.19a and 19b show both frequency responses of Fig.18a and 18b in the time domain for a  $P_{SET}$  sinusoidal pressure signal with frequency  $f = 0.1$  Hz, average value  $A_V = 3$  bar rel and amplitude  $A = 2$  bar rel. Likewise to the diagrams of Fig.20 and still referring to the Bode diagrams of Fig.18, the frequency responses in the time domain for a  $P_{SET}$  with frequency  $f = 1.5$  Hz are shown respectively in Fig.20a and 20b for  $T = 50$  ms and  $T = 100$  ms.

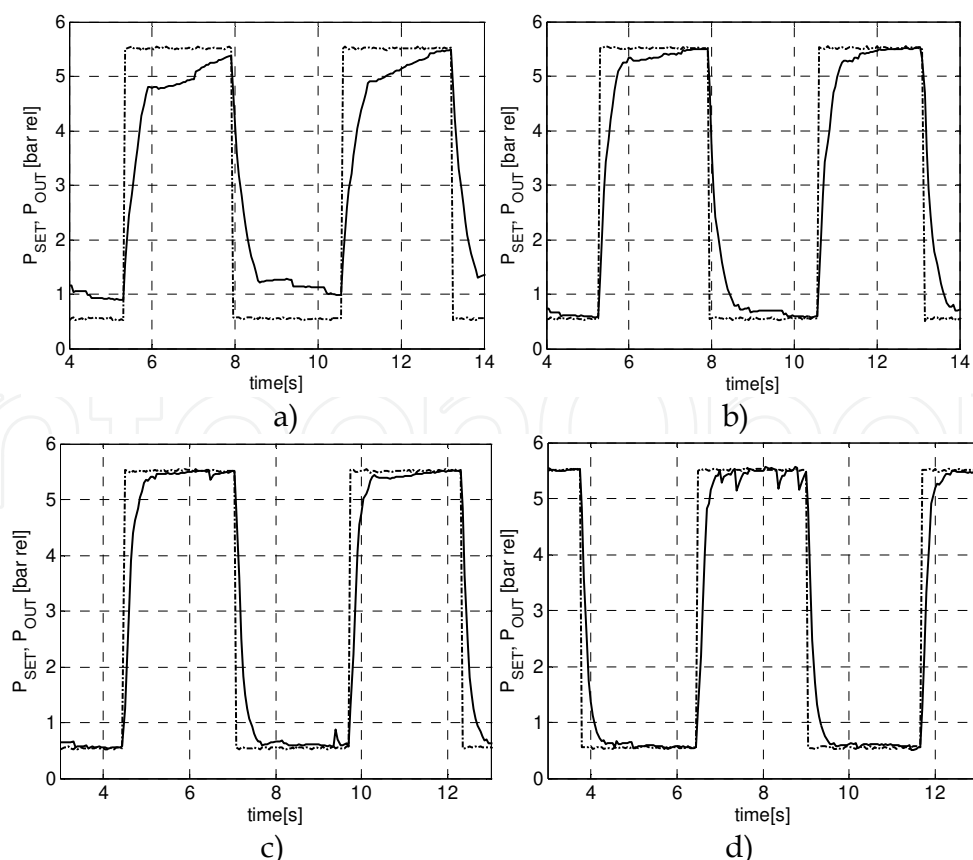


Fig. 17. Effects of the proportional gain: a)  $K_p = 0.3$ ; b)  $K_p = 0.9$ ; c)  $K_p = 1.8$ ; d)  $K_p = 2.4$ .

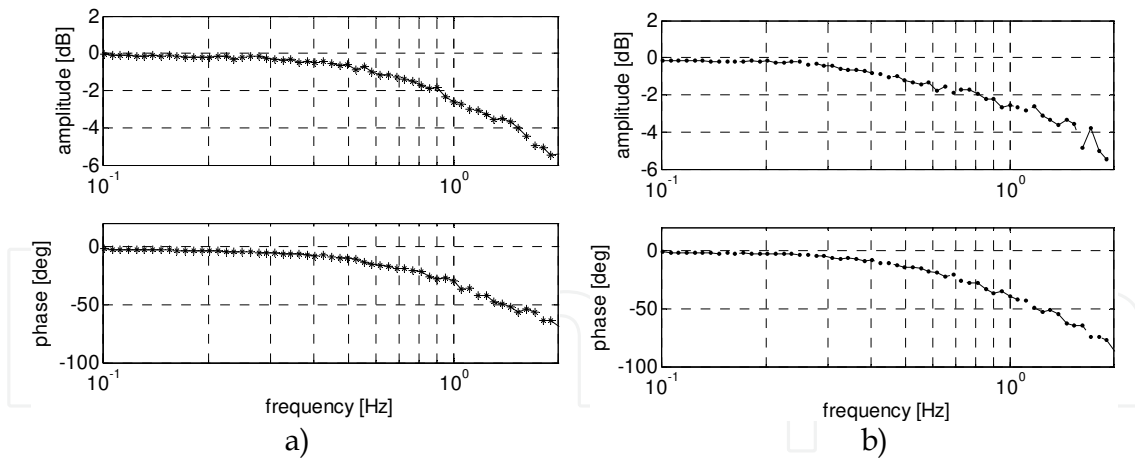


Fig. 18. Closed-loop frequency responses of the proposed pressure control system for different periods of the PWM modulation; a)  $T = 50$  ms; b)  $T = 100$  ms.

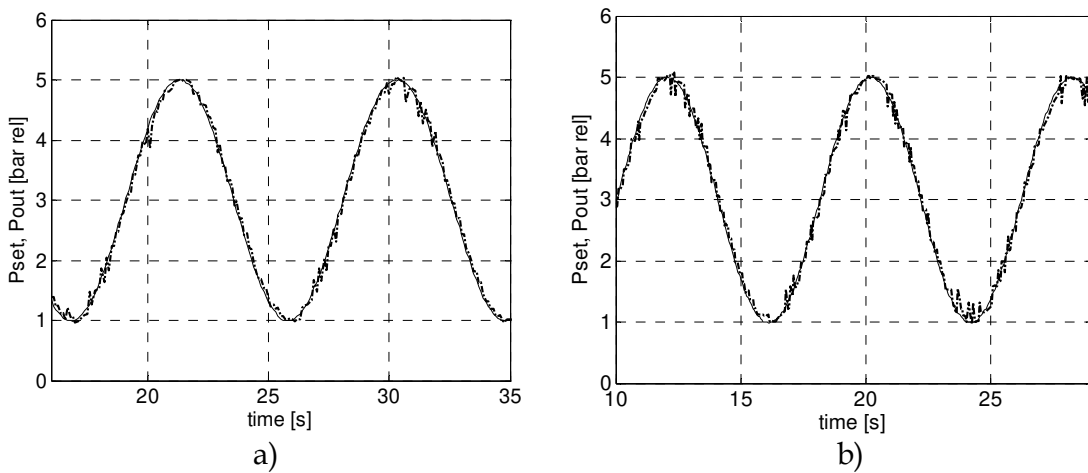


Fig. 19. Frequency responses in the time domain for a sinusoidal  $P_{SET}$  with  $f = 0.1$  Hz,  $A_v = 3$  bar rel and  $A = 2$  bar rel: a)  $T = 50$  ms; b)  $T = 100$  ms.

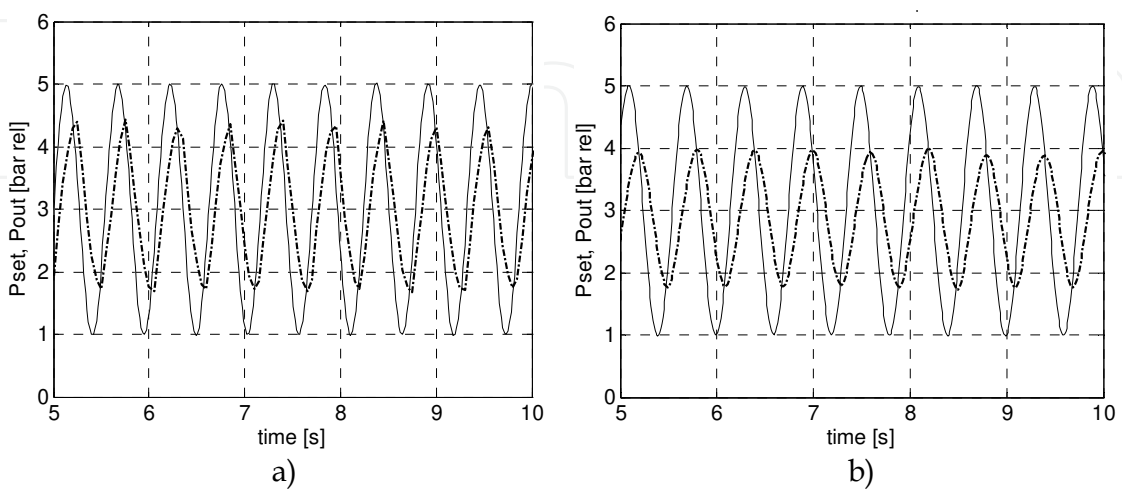


Fig. 20. Frequency responses in the time domain for a sinusoidal  $P_{SET}$  with  $f = 1.5$  Hz,  $A_v = 3$  V and  $A = 2$  V: a)  $T = 50$  ms; b)  $T = 100$  ms.



#### 4. The CaUMHa underactuated robotic hand: overall design

According to the mechatronic design proposed and described in Sections II and III, a prototype of Ca.U.M.Ha. robotic hand has been built and tested by using the experimental test-bed of Fig. 21, which shows: 1) Ca.U.M.Ha. robotic hand prototype; 2) pneumatic cylinder; 3) PWM modulated pneumatic digital valves; 4) 3/2 pneumatic digital valve; 5) 5/2 pneumatic digital valve; 6) external block SCB-68; 7) electronic board to convert the signal  $V_{PWM}$  to  $V_{PWM 1}$  and  $V_{PWM 2}$ ; 8) electronic board to control the thumb of the robotic hand.

The mechanical parts of Ca.U.M.Ha., i.e. underactuated fingers along with their linkage systems, palm and thumb, have been manufactured in aluminum, while the tank is made by steel.

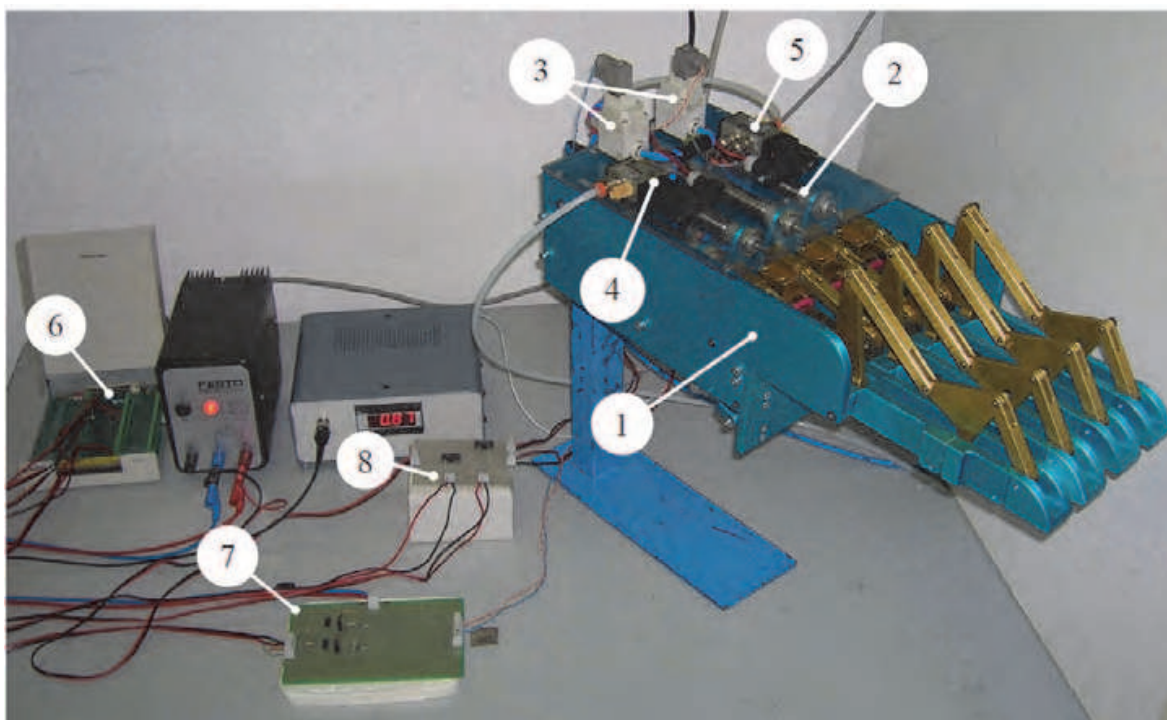


Fig. 21. Prototype and experimental test-bed of the Ca.U.M.Ha. robotic hand, 1) Ca.U.M.Ha. robotic hand; 2) double-acting pneumatic cylinder; 3) two PWM modulated pneumatic digital valves; 4) 3/2 pneumatic digital valve; 5) 5/2 pneumatic digital valve; 6) terminal block SCB-68; 7) electronic board to split and amplify at 24 V the control signals  $V_{PWM 1}$  and  $V_{PWM 2}$ ; 8) electronic board to split and amplify at 24 V both signals to control the thumb of the robotic hand.

#### 5. Conclusions

In this Chapter the mechatronic design has been reported for the Ca.U.M.Ha. (Cassino-Underactuated-Multifinger-Hand) robotic hand. In particular, the underactuation concept is addressed by reporting several examples and kinematic synthesis and the mechatronic design have been developed for a finger mechanism of the robotic hand. As a result the Ca.U.M.Ha. robotic hand shows a robust and efficient design, which gives good flexibility and versatility in the grasping operation at low-cost. The kinematic synthesis and



optimization of the underactuated finger mechanism of Ca.U.M.Ha. have been formulated and implemented. In particular, two function-generating four-bar linkages and one offset slider-crank mechanism have been synthesized by using the Freudenstein' equations and optimizing the force transmission, which can be considered as a critical issue because of the large rotation angles of the phalanxes. A closed-loop pressure control system through PWM modulated pneumatic digital valves has been designed and experimentally tested in order to determine and analyze its static and dynamic performances. The proposed and tested closed-loop control system is applied to the Ca.U.M.Ha. robotic hand in order to control the actuating force of the pneumatic cylinders of the articulated fingers. Consequently, a force control of the grasping force has been developed and tested according to a robust and low-cost design of the robotic hand.

## 6. References

- Angeles J., Bernier A., (1987). The Global Least-Square Optimization of Function Generating Linkages. *Journal of Mechanisms, Transmissions and Automation in Design*, Vol.109, pp.204-209.
- Arimoto S., (2003). Control for a family of nonlinear and under-actuated systems with DOF-redundancy and geometric constraints, *SICE Annual Conference in Fukui*, Fukui, pp.2205-2210.
- Banks J.L. (2001). Design and control of an anthropomorphic robotic finger with multi-point tactile sensation MS Thesis, MIT, Cambridge.
- Beccai L., Roccella S., Ascari L., Valdastrì P., Sieber A., Carrozza M. C., Dario P., (2009). Development and experimental analysis of a soft compliant tactile microsensor for anthropomorphic artificial hand. *IEEE/ASME Transaction on Mechatronics*, Vol.13, no.2, pp.158-168.
- Belforte G., Mauro S., Mattiazzo G.(2004). A method for increasing the dynamic performance of pneumatic servosystems with digital valves, *Mechatronics*, Vol.14 pp. 1105-1120.
- Belforte, G.; Mattiazzo, G.; Mauro, S. & Cocito, C. (2001). A robotic system for apples harvesting. *10<sup>th</sup> RAAD International Workshop on Robotics in Alpe-Adria-Danube Region*, Vienna, paper: RD-103.
- Bicchi A., (2000). Hands for Dexterous Manipulation and Robust Grasping: a Difficult Road Toward Simplicity. *IEEE/ASME Transaction on Robotics and Automation*, Vol.16, n.6, pp.652-662.
- Birglen L., Gosselin C.M., (2003). On the Force Capability of Underactuated Fingers. *Proceedings of the 2003 IEEE International Conference on Robotics and Automation, ICRA 2003*, Taipei, pp.1139-1145.
- Birglen L., Gosselin C.M., (2004). Kinetostatic analysis of underactuated fingers, *IEEE Transactions on Robotics and Automation*, Vol.20, n.2 pp. 211-221.
- Birglen L., Gosselin C.M., (2005). Fuzzy Enhanced Control of an Underactuated Finger Using Tactile and Position Sensors. *Proceedings of the 2005 IEEE International Conference on Robotics and Automation, ICRA 2005*, Barcelona, pp.2320-2325.
- Bulanon, D.M.; Kataoka, T.; Ota, Y. & Hiroma, T. (2001). A machine vision system for the apple harvesting robot. *Agricultural Engineering International: the CIGR J. of Scientific Research and Development*, Vol.3, paper: PM 01 006.

- Butterfas J., Grebenstein M., Liu H., Hirzinger G. (2001). DLR hand II: Next Generation of a Dextrous Robot Hand. *Proceedings of the 2001 IEEE International Conference on Robotics and Automation, ICRA 2001*, Seoul, pp.109-114.
- Carrozza M.C., Massa B., Micera S., Lazzarini R., Zecca M. e Dario P. (2002). The Development of a Novel Prosthetic Hand Ongoing Research and Preliminary Results. *IEEE/ASME Transaction on Mechatronics*, Vol.7, n.2, pp.108-114.
- Casolo F., Lorenzi V., (1990). Criteri di scelta e Ottimizzazione di Modelli per la Simulazione del Dito Umano. *X Congresso Nazionale dell'Associazione Italiana di Meccanica Teorica ed Applicata (AIMETA-90)*, Pisa, pp.415-420.
- Chevallereau C., Grizzle J.W., Moog C.H., (2004). Non Linear Control of Mechanical Systems with One Degree of Underactuation. *Proceedings of the 2004 IEEE International Conference on Robotics and Automation, ICRA 2004*, New Orleans, pp.2222-2228.
- Crisman J.D., (1996). Robot Arm End Effector, 1996. US Patent n. 5570920.
- Figliolini G., Ceccarelli M. (2002) A novel articulated mechanism mimicking the motion of index fingers, *Robotica*, Vol.20, pp.13-22.
- Figliolini G., Rea P.(2003) Ca.U.M.Ha. robotic hand for harvesting horticulture products, *XXX CIOSTA - CIGRV Congress on Management and Technology Applications to Empower and Agro-Food Systems*, Turin, pp.288-295.
- Figliolini, F. & Rea, P. (2004). Actuation Force Control of Ca.U.M.Ha. Robotic Hand Through PWM Modulated Pneumatic Digital Valves. *3<sup>rd</sup> FPNI - PhD Symposium on Fluid Power*, Terrassa, pp. 149-156.
- Figliolini, G. & Rea, P. (2005). Synthesis and optimization of an underactuated finger mechanism, *Proceedings of the 9th IFToMM Symposium on Theory of Machines and Mechanisms (SYROM'05)*, Bucharest, Vol.3, pp. 747-752.
- Figliolini, G. & Rea, P. (2006). Overall design of Ca.U.M.Ha. robotic hand, *Robotica*, Vol.24 n.3, pp. 329-331.
- Figliolini G. & Rea, P. (2007). Ca.U.M.Ha. Robotic Hand (Cassino-Underactuated-Multifinger-Hand). *Proceedings of the 2007 IEEE/ASME International Conference on Advanced Intelligent Mechatronics (AIM2007)*, Zurich, paper number 250.
- Figliolini G., Rea P., Principe M.(2003). Mechatronic design of Ca.U.M.Ha (Cassino-Underactuated-Multifinger-Hand), *12th RAAD Workshop on Robotics in Alpe-Adria-Danube Region, Cassino*, paper: 026RAAD03.
- Francisco J. V. C., (2000). Applying principles of robotics to understand the biomchanics, neuromuscular control and clinical rehabilitation of human digits. *Proceedings of the 2000 IEEE International Conference on Robotics and Automation, ICRA 2000*, San Francisco, pp.270-275.
- Freudenstein F.,(1955). Approximate synthesis of four-bar linkages, *Transactions of the ASME*, Vol. 77, pp.853-861.
- Gokhale K., Kawamura A. and R.G. Hoft, (1987).Dead beat microprocessor control of PWM inverter for sinusoidal output waveform synthesis *IEEE/ASME Transaction on Industry application*, Vol.1A 23, no.5, pp.901-910.
- Gosselin C., Angeles J., (1989). Optimization of Planar and Spherical Function Generators as Minimum-Defect Linkages. *Mechanism and Machine Theory*, Vol.24, pp.293-307.

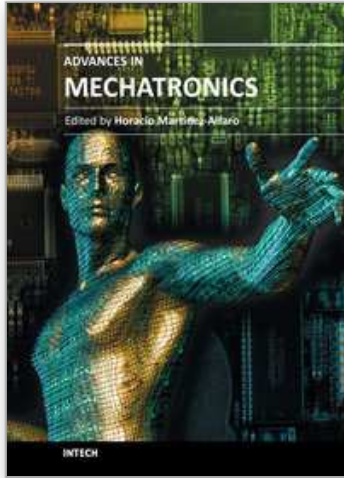
- Haulin E.N., Lakis A.A., Vinet R., (2001). Optimal Synthesis of a Planar Four-Link Mechanism used in a Hand Prosthesis, *Mechanism and Machine Theory*, Vol.36, pp.1203-1214.
- Haulin E.N., Vinet R., (2003). Multiobjective Optimization of Hand Prosthesis Mechanisms *Mechanism and Machine Theory*, Vol.38, pp.3-26.
- Imai Y., Namiki A., Hashimoto K., Ishikawa M., (2004). Dynamic Active Catching Using a High-speed Multi-fingered Hand and a High-speed Vision System. *Proceedings of the 2004 IEEE International Conference on Robotics and Automation, ICRA, New Orleans*, pp.1849-1854.
- Jiang L., Sun D. and Liu H., (2009). An inverse-kinematics table-based solution of a humanoid robot finger with nonlinearly coupled joints *IEEE/ASME Transaction on Mechatronics*, Vol.14, n.3, pp.273-281.
- Jacobsen, S.C.; Wood, J.E.; Knutti, D.F. & Biggers, K.B. (1984). The Utah/MIT dexterous hand: work in progress, *The Int. J. of Robotics Research*, Vol.3, No.4, pp. 21-50.
- Jobin J.P., Buddenberg H.S., Herder J.L., (2004). An Underactuated Prosthesis Finger Mechanism with Rolling Joints. *Proceedings of DETC ASME, 28th Biennial Mechanisms Conference, Salt Lake City*,
- Kim K., Edward Colgate J., Santos-Munné J.J., Makhlin A. and Peshkin M., (2010). On the design of miniature haptic devices for upper extremity prosthetics. *IEEE/ASME Transaction on Mechatronics*, Vol.15, n.1, pp.27-39.
- Lalibertè, T., Gosselin, C.M. (1998). Simulation and design of underactuated mechanical hands. *Mechanism and Machine Theory*, Vol.33, No.1, pp.39-57.
- Lalibertè T., Birglen L., Gosselin C.M. (2002). Underactuation in robotic grasping hands, *Japanese Journal of Machine Intelligence and Robotic Control*, Vol.4, n.3 pp.77-87.
- Lee H.J., Yi B.J., Oh S.R., Suh I.H., (2001). Optimal Design and Development of a Five-Bar Finger with Redundant Actuation, *Mechatronics*, Vol. 11, pp.27-42.
- Liu, H.; Butterfass, J.; Knoch, S.; Meisel, P. & Hirzinger, G. (1999). A new control strategy for DLR's multisensory articulated hand. *IEEE Control systems*, Vol.19, n.2, pp.47-54.
- Liu G. and Li Z., (2004). Real time grasping-force optimization for multifingered manipulation: Theory and experiments *IEEE/ASME Transaction on Mechatronics*, Vol.9, n.1, pp.65-77.
- Liu H., Meuse P., Hirzinger G., Jin M., Liu Y., and Xie Z. (2008).The modular multisensory DLR-HIT-hand: Hardware and software architecture *IEEE/ASME Transaction on Mechatronics*, Vol.13, n.4, pp.461-469.
- Liu H., Wu K., Meusel P., Seitz N., Hirzinger G., Jin M.H., Liu Y.W., Fan S.W., Lan T. and Chen Z.P. (2008). Multisensory five-finger dexterous hand: The DLR/HIT hand II *IEEE/RSJ International Conference on Intelligent Robots and Systems*. Acropolis Convention Center Nice, Sept, 22-26.
- Lotti F., Tiezzi P., Vassura G., Biagiotti L., Melchiorri C., Palli G., (2004). UBH 3: A Biologically Inspired Robotic Hand. *Proc. of IEEE International Conference on Intelligent Manipulation and Grasping (IMG 04)*, Genova, pp. 39-45.
- Luo M., Mei T., Wang X., Yu Y., (2004). Grasp Characteristics of an Underactuated Robot Hand. *Proceedings of the 2004 IEEE International Conference on Robotics and Automation, ICRA 2004, New Orleans, (USA)*, pp.2236-2241.
- Mason M. T., Salisbury J.K., (1984). Robot hand and the mechanics of manipulation, Tokyo, pp.151-167.

- Mason, M.T. & Salisbury, J.K. (1985). *Robot Hand and the Mechanics of Manipulation*, MIT Press, Cambridge, MA.
- Montambault, S. & Gosselin, C.M. (2001). Analysis of underactuated mechanical grippers. *ASME J. of Mechanical Design*, Vol.123, n.3, pp. 39-57.
- Namiki A., Imai Y., Ishikawa M., Kaneko M. (2003). Development of a High-Speed Multifingered Hand System and Its Application to Catching. *Proceedings of the 2003 IEEE/RSJ Intl. Conference on Intelligent Robots and Systems*, Las Vegas, pp.2666-2671.
- Raparelli, T.; Mattiazzo, G. & Mauro, S., Velardocchia M. (2000). Design and development of a pneumatic anthropomorphic hand. *J. of Robotic Systems*, Vol.17, n.1, pp. 1-15.
- Rash G.S., Belliappa P.P., Wachowiak M.P., Somia N.N., Gupta A., (1999). A Demonstration of the Validity of a 3-D Video Motion Analysis Method for Mesuring Finger Flexion and Extension, *Journal of Biomechanics*, 32, pp.1337-1341.
- Rea P., (2007). Mechatronic Design of underactuated robotic hand with pneumatic actuation, Ph.D. Dissertation, University of Cassino, Cassino. Available at: <http://www.scuoladottoratoingegneria.unicas.it/Tesi/Ciclo XIX/TesiRea.pdf>
- Schultz S., Pylatiuk C., Bretthauer G., (2001). A New Ultralight Anthropomorphic Hand. *Proceedings of the 2001 IEEE International Conference on Robotics and Automation, ICRA 2001*, Seoul, (Korea), pp.2437-2441.
- Schweizer A., Frank O., Ochsner P.E., Jacob H.A.C., (2003). Friction Between human Finger Tendons and Pulleys at High loads, *Journal of Biomechanics*, 36, pp.63-71.
- Sorli M., Figliolini G., Pastorelli S., Modeling and experimental validation of a two-way pneumatic digital valve, *Bath Workshop on Power Transmission & Motion Control*, Eds. C.R. Barrows and K.A. Edge, Professional Engineering Publishing, London, 2003, pp.291-305.
- Sorli M., Figliolini G. and Pastorelli S., (2004). Dynamic model and experimental investigation of a pneumatic proportional pressure valve. *IEEE/ASME Transaction on Mechatronics*, Vol.9, n.1, March 2004, pp.78-86.
- Su F-C., Kuo L.C., Chiu H.Y., Chen-Sea M.J., (2003). Video-Computer Quantitative Evaluation of Thumb Function using Workspace of the Thumb. *Journal of Biomechanics*, Vol.36, pp.937-942.
- Salisbury J. K., Craig J. J., (1981). Articulated Hands: Force Control and Kinematic Issues. *Joint Automatic Control Conference*, Charlottesville, pp.17-19.
- Sutherland G., Roth B., (1973). A Transmission Index for Spatial Mechanisms. *ASME Journal of Engineering Industry*, pp.589-597.
- Stellin G., Cappiello G., Roccella S., Carrozza M.C., Dario P., Metta G., Sandini G., Becchi F., (2006). Preliminary Design of an Anthropomorphic Dexterous Hand for a 2-Years-Old Humanoid: Towards Cognition. *The First IEEE/RAS-EMBS International Conference on Biomedical Robotics and Biomechatronics*, pp.290-295.
- Taylor C.L., Schwartz R.J., (1955). The Anatomy and Mechanics of the Human Hand. *Artificial Limbs*, Vol.2 pp.22-35.
- Van Varseveld R. B. and Bone G. M.,(1997). Accurate position control of a pneumatic actuator using On/Off solenoid valves *IEEE/ASME Transaction on Mechatronics*, Vol.2, n.3, pp.195-204.
- Wenzeng Z., Chen Q., Sun Z., Khao D., (2004). Passive Adaptive Grasp Multi-Fingered Humanoid Robot Hand with High Under-actuated Function. *Proceedings of the 2004*

- IEEE International Conference on Robotics and Automation, ICRA 2004, New Orleans, pp.2222-2228.*
- Yamano I., Maeno T., (2005). Five Fingered Robot Hand using Ultrasonic Motors and Elastic Elements. *Proceedings of the 2005 IEEE International Conference on Robotics and Automation*, pp.2673-2678.
- Yuan X., Stemmler H. and I. Barbi (2001). Self-balancing of the clamping-capacitor-voltages in the multilevel capacitor-clamping-inverter under sub-harmonic PWM modulation *IEEE/ASME Transaction on Power Electronics*, Vol.16, n.2, pp.256-263.
- Yun M.H., Eoh H.J., Cho J., (2002). A Two Dimensional Dynamic Finger Modeling for the Analysis of Repetitive Finger Flexion and Extension, *Journal of Industrial Ergonomics*, Vol.29, pp.231-248.

IntechOpen





### **Advances in Mechatronics**

Edited by Prof. Horacio Martinez-Alfaro

ISBN 978-953-307-373-6

Hard cover, 300 pages

**Publisher** InTech

**Published online** 29, August, 2011

**Published in print edition** August, 2011

Numerous books have already been published specializing in one of the well known areas that comprise Mechatronics: mechanical engineering, electronic control and systems. The goal of this book is to collect state-of-the-art contributions that discuss recent developments which show a more coherent synergistic integration between the mentioned areas. The book is divided in three sections. The first section, divided into five chapters, deals with Automatic Control and Artificial Intelligence. The second section discusses Robotics and Vision with six chapters, and the third section considers Other Applications and Theory with two chapters.

#### **How to reference**

In order to correctly reference this scholarly work, feel free to copy and paste the following:

Pierluigi Rea (2011). On the Design of Underactuated Finger Mechanisms for Robotic Hands, *Advances in Mechatronics*, Prof. Horacio Martinez-Alfaro (Ed.), ISBN: 978-953-307-373-6, InTech, Available from: <http://www.intechopen.com/books/advances-in-mechatronics/on-the-design-of-underactuated-finger-mechanisms-for-robotic-hands>

**INTECH**  
open science | open minds

#### **InTech Europe**

University Campus STeP Ri  
Slavka Krautzeka 83/A  
51000 Rijeka, Croatia  
Phone: +385 (51) 770 447  
Fax: +385 (51) 686 166  
[www.intechopen.com](http://www.intechopen.com)

#### **InTech China**

Unit 405, Office Block, Hotel Equatorial Shanghai  
No.65, Yan An Road (West), Shanghai, 200040, China  
中国上海市延安西路65号上海国际贵都大饭店办公楼405单元  
Phone: +86-21-62489820  
Fax: +86-21-62489821



© 2011 The Author(s). Licensee IntechOpen. This chapter is distributed under the terms of the [Creative Commons Attribution-NonCommercial-ShareAlike-3.0 License](#), which permits use, distribution and reproduction for non-commercial purposes, provided the original is properly cited and derivative works building on this content are distributed under the same license.

IntechOpen

IntechOpen